MODELING URBAN EXPANSION IN VIETNAM USING TIME SERIES LANDSAT

BY

LI XI

BA, Binghamton University, 2016

THESIS
Submitted in partial fulfillment of the requirements for
the degree of Master of Arts in Geography
in the Graduate School of
Binghamton University
State University of New York
2019

Accepted in partial fulfillment of the requirements for
The degree of Master of Arts in Geography
In the Graduate School of
Binghamton University
State University of New York
2019

May 3, 2019

Chengbin Deng, Chair and Faculty Advisor
Department of Geography, Binghamton University

Mark Reisinger, Member
Department of Geography, Binghamton University

Mark Blumler, Member
Department of Geography, Binghamton University

Abstract

Ho Chi Minh City Metropolitan Area (HCMA) has undergone tremendous urban expansion in the last several decades. To quantify its long-lasting urban growth, an objective and repeatable method was proposed using all available Landsat between 2000 and 2017. Therefore, time series impervious surface cover fractions were estimated for the HCMA area on the basis of sub-pixel analysis. Sub-pixel methods can successfully be applied upon the heterogeneous urban landscape, while per-pixel methods can only assign one image pixel to one urban land cover category. The proposed methodology in this study not only produced an impervious surface fraction cube which demonstrates time series urban expansion at HCMA area, but also depicted long-term urban trajectories with a four-parameter logistic model. This selected logistic model was utilized to delineate a complete urban evolution trajectory between 2000 and 2017. Moreover, a different logistic model was used to show urban expansion density variations over distance from the urban core. Important results have been generated from the proposed method. First, the central urban density of HCMA continued to increase between 2000 and 2017 and caused great impacts in its surrounding provinces, including Binh Duong, Dong Nai, and Long An. A significant number of agricultural lands have been converted into urban land during intensive urban sprawl. This continuing urban sprawl has also prospered several cities adjacent to the Ho Chi Minh City in the HCMA area, including Bien Hoa City, Thu Dau Mot City, and Tan An City. Time series modeled impervious surface cover fractions were used to compare with the reference samples for accuracy

assessments. The best MAE, SE, RMSE and adjusted R^2 are 4.73%, 0.81%, 5.52%, and 0.85. The accuracy of the adopted sub-pixel mapping method is comparable to, or even better than those of previous studies. Moreover, time series urban trajectory of HCMA area demonstrated a typical three-stage urban transition process, including the pre-change stage, change stage with an increase in impervious surface, and the post-change stage with saturated impervious surface. Green vegetation space has been often transformed into the impervious surface during urban sprawl. Further, the urban expansion density analysis shows that impervious surface density continued to decrease as distance decayed from the center but continued to increase over HCMA area between 2000 and 2017. In actuality, the urban density has increased over HCMA area in the temporal domain but decreased in the spatial domain. Overall, the proposed method provided an objective and repeatable means to estimate time series urban expansion, evolution, and density changes at the HCMA area in the 2000-2017 period.

Acknowledgements

I want to thank my advisor, Dr. Chengbin Deng for his inspirational advice and guidance. I am also extremely grateful to the support of my committee members: Dr. Mark E. Reisinger and Dr. Mark A. Blumler. I also want to thank all faculty and staff members of the Geography Department at Binghamton University for their generous help during my undergraduate and graduate educations. Finally, I want to thank my parents for their endless amounts of love and support.

Table of Contents

List of Tables

List of Figures

List of Abbreviations

ETM+	Enhanced Thematic Mapper Plus
Fig	Figure
HCMA	Ho Chi Minh City Metropolitan Area
LASRC	Landsat Surface Reflectance Code
LEADPS	Landsat Ecosystem Disturbance Adaptive Processing System
MAE	Mean Absolute Error
OLI	Operational Land Imager
RMSE	Root Mean Squared Error
SE	Systematic Error
TM	Thematic Mapper
UN	United Nations
USGS	United States Geological Survey
WRS-2	Worldwide Reference System
UTM	Universal Transverse Mercator grid system
WGS84	World Geodetic System 1984

1. Introduction

Urban expansion becomes a major concern in rapidly urbanizing areas due to considerable loss of tropical forests (DeFries et al., 2010), cultivated areas (Bren d'Amour et al., 2017), and biodiversity hotspots (Seto, Guneralp, & Hutyra, 2012). Deforestation contributes to atmospheric carbon emission as the second largest source on the Earth, following fossil fuel consumption (Van der werf et al., 2009). Currently, the tropical region has relatively the highest deforestation rate (Sodhi et al., 2004). Moreover, fifty global cities' urban expansion is found to be negatively associated with their cultivated land resources (Bagan & Yamagata, 2014). Additionally, urban expansion is one of the major drivers of species extinction and biotic homogenization (Mckinney, 2006). Hence, there has been an urgent need to build a comprehensive understanding of how urbanization evolves and develops over time (Seto & Shepard, 2009).

In Asia, for example, numerous natural lands have been converted for urban and residential developments in recent decades. Rapid urban expansion occurring in metropolitan regions is projected to cause the highest absolute decrease in productive cultivated areas in Asia by 2030 (Bren d'Amour et al., 2017). Moreover, the world's urban population is predicted to reach 68% by 2050 with most of them in Asia, based on the records of the United Nations Department of Economic and Social Affairs (UN, 2018). In the next twenty years, Asia is also estimated to have the highest amount of urban population, compared with other developing regions (Montgomery, 2008). Accurate and current information is needed to address this urban sprawl issue for urban and environmental planning, policy, and decision-making processes (Ridd,

1995). Therefore, time series Landsat (2000-2017) was utilized to study urban expansion and land cover changes for the most populated area in Vietnam, Ho Chi Minh City Metropolitan Area.

The urban population in Vietnam has increased from 19.5% to 30% in the 1990-2009 period (World Bank, 2012). The proportion of urban inhabitants is projected to exceed the rural residents by 2040 due to urban sprawl (UN, 2008). Despite this tremendous urbanization progress, the long-term spatial extent of the increase in impervious surface cover fractions remains unexplored. Impervious surfaces are the most significant component of urban composition through anthropogenic activities. Impervious surfaces include building rooftops, sidewalks, roads, and other impenetrable pavements (Arnold & Gibbons, 1996). It is acknowledged as an important environmental indicator due to its significant hydrological, physical and water quality impacts (Schuler 2003; Chabaeva, Civco & Hurd, 2009). Impervious surface has direct effects on local hydrological systems by increasing surface runoff volumes and streamflow discharge rates and decreasing baseflow and groundwater recharge (Jennings and Jarnagin 2000; Burns et al., 2005). This eventually leads to increasing flood frequency and magnitude (Arnold et al., 1982; Moscrip & Montgomery, 1997). Moreover, higher air and ground temperatures occurring above the non-evaporating impervious surface contributes to rising water temperatures (Schuler, 1994). As a consequence, substantial aquatic animal and plant populations are severely endangered from rapid warming of living environments (Gilles et al., 2003; Miltner et al., 2004; Melesse and Wang, 2008). Further, increasing stormwater runoff transports heavy loads of non-point source environmental pollutants into local watershed systems (Sartor & Boyd, 1972; Young et al., 1989; Novotny 1994; Gnecco et al., 2005). This accelerated water contamination from impervious surface pavements deteriorate and degrade local water

quality (Brabec, Schulte & Richards, 2002; Tong & Chen, 2002; Mallin et al., 2000). Hence, understanding and monitoring urban impervious surface is essential for watershed ecosystem management and protection.

Remote sensing technologies provide flexible and useful tools to geographers and planners in monitoring and quantifying urban impervious surface. To enable a more accurate estimation of urban impervious surface dynamics, it is essential to incorporate spatial and temporal contexts from remote sensing techniques (Powell et al., 2008; Deng & Zhu, 2018). Considering the spatial context, traditional classification algorithms usually assign one land use and land cover class to an image pixel (Taubenböck et al., 2012; Schneider et al., 2015). These conventional per-pixel classification methods are inherently not suitable for mapping the urban heterogeneous landscape in which one pixel may contain several land cover types. Therefore, enormous research efforts have been devoted to monitoring urban impervious surface distribution at a sub-pixel level to solve the mixed-pixel problem. Generally, the sub-pixel classification has been implemented to identify the areal proportion of impervious surface in each pixel instead of categorizing a complete pixel to an urban-related class. The conceptual V-I-S (vegetation-impervious surface-soil) model proposed by Ridd (1995) parameterized important biophysical components in the complex urban environment. Further studies have extended the V-I-S model foundation in various spectral mixture analysis (SMA) to optimize mapping accuracies (Ward, Phinn & Murray, 2000; Wu, 2004; Powell et al., 2007; Lu, Moran & Hetrick, 2011; Deng & Wu, 2013a). Moreover, a robust and reliable cubist regression tree algorithm was developed to map impervious surfaces for each 5-year period between 2001 and 2011 National Land Cover Dataset (NLCD) over the conterminous United States (Yang et al., 2003a; Xian & Homer, 2010; Homer et al., 2015). One particular study integrates SMA and several machine learning methods,

including cubist regression tree and random forest, to generate comparable sub-pixel imperviousness mapping results (Deng & Wu, 2013b). Random forest is gaining more popularity in recent studies for estimating urban imperviousness due to its robustness against overfitting (Tsutsumida, et al., 2016; Deng et al., 2017; Deng & Zhu, 2018). However, despite the active progress of sub-pixel urban imperviousness mapping approaches, insufficient acquisition of temporal information can result in missing of a significant clue about the land cover.

Considering the temporal context, a substantial body of urban literature have only derived fractional impervious surface information at one point (Yang et al., 2003a; Xian, Crane & Su, 2006; Yuan & Bauer, 2007) and/or multiple points in time (Yang et al., 2003b; Xian & Crane, 2005; Xian, Crane & McMahon, 2008; Powell et al., 2008; Shahtahmassebi et al., 2016). Sub-pixel imperviousness classifications of one-time point usually reveal the urban spatial extent within one individual year, while multiple-time-point studies often leverage temporal information from a long-term remotely sensed imagery archive (e.g. Landsat) to provide more explicit quantification of urban imperviousness changes. Yang et al. (2003b), Xian and Crane (2005), Xian, Crane & McMahon (2008), Xian and Homer (2010) all utilized the cubist regression-tree algorithm to detect urban land cover change for two or more dates at various geographical scales across the United States. Powell et al. (2008) applied SMA to estimate 1972 and 2006 percent impervious surface within a Water Resources Inventory Area. Shahtahmassebi et al. (2016) created a framework combining MESMA and other techniques for summarizing urban expansion and re-densification mechanisms within a Chinese city for every seven years between 1995 and 2009. However, important inter-annual details of urban land cover changes are omitted from stable- or multiple-time-point studies. It is also worth noting that compounded errors can occur from sub-pixel mapping for different time points (Zhu, 2017). Consequently, a

dense stack of satellite time series becomes an appropriate and preferable solution for detecting long-term and continuous changes of impervious surface distribution.

To observe and record the complexities of urbanization, studying time series trajectory of urban proportion imperviousness based on historical satellite imagery collection has become more and more popular. Specifically, more recent studies are found to use higher frequencies of Landsat time series (Zhu, 2017). While there is no widely accepted definition for time series, it can generally be defined as long term and continuous fields. In this study, the discussion of time series studies was further limited to sub-pixel urban impervious mapping products generated at an annual frequency. Given these constraints, substantially fewer studies were found belong to the time series category whereas more research concentrated on urban land cover classifications (Li, Gong & Lu, 2015; Li et al., 2018) or natural ecosystem dynamics (Zhu & Woodcock, 2014; Roberts, King & Davies, 2015; Bullock, Woodcock & Olofsson, 2018; Roy & Yan, 2019). Nevertheless, a few applications focused on the urban domain with time series Landsat. For example, Sexton et al. (2013) employed an empirical method to retrieve annual, long-term continuous fields of impervious surface cover in the Washington DC - Baltimore metropolitan region from 1984 to 2010. Its follow-up study Song et al. (2016) applied a post-classification method to characterize the magnitude, timing, and duration of urban expansion based on the resulting annual, fractional impervious surface cover dataset of Sexton et al. (2013). Time series urban growth trajectories over the Washington DC-Baltimore metropolitan region were monitored to characterize continuous fields of impervious surface cover changes. Thus, in order to demonstrate annual and long-term urban transition patterns in the continuous fields, decadal observations at high frequency (e.g. annual) are required.

In this study, an objective and repeatable method was proposed for mapping time series impervious surface cover fractions using all available Landsat between 2000 and 2017. The introduced post-classification method from Song et al. (2016) was further established to study a complete urban growth process over the HCMA area. Urban expansion density variations were also estimated and analyzed with modellng techniques. In general, both spatial and temporal contexts were considered in the research progress.

2. Conceptualization Model and Hypotheses

Significant concepts in this study consist of urban expansion, imperviousness change, urban evolution and urban expansion density variation. The impervious surface cover is the most important member of urban composition. During urban expansion, impervious surface cover continues to increase at the expense of natural lands, especially agricultural lands surrounding the suburban area. Moreover, long-term urban expansion reveals a comprehensive view of urban evolution of a city. Therefore, it is highly necessary to monitor and analyze urban evolution for a better understanding of time series urban sprawl impacts. Further, as the urban area continues to grow towards the boundary, the acquisition of information about urban expansion density over varying distances from the urban core becomes essential. The relationship between percent imperviousness and distance from the urban core can be understood carefully based on the corresponding density analysis. Fig. 1 shows the conceptualization model.

Several sets of null (Ho) and alternative hypotheses (Ha) were introduced and tested in this study. These hypotheses, which were drawn from extensive literature reviews about urban growths and imperviousness changes, include:

Ho 1: Random forest model is not a reliable and robust algorithm for mapping impervious surface cover at a sub-pixel spatial scale and time-series temporal level.

Ha 1: Random forest model is a reliable and robust algorithm for mapping impervious surface cover at a sub-pixel spatial scale and time-series temporal level.

Ho 2: The HCMA area does not become increasingly expanded between 2000 and 2017.

Ha 2: The HCMA area becomes increasingly expanded between 2000 and 2017.

Ho 3: Urban expansion process over the HCMA area cannot be demonstrated using a logistic model.

Ha 3: Urban expansion process over the HCMA area can be demonstrated using a logistic model.

Ho 4: There is not a close relationship between urban expansion density and distance at the HCMA area.

Ha 4: There is a close relationship between urban expansion density and distance at the HCMA area.

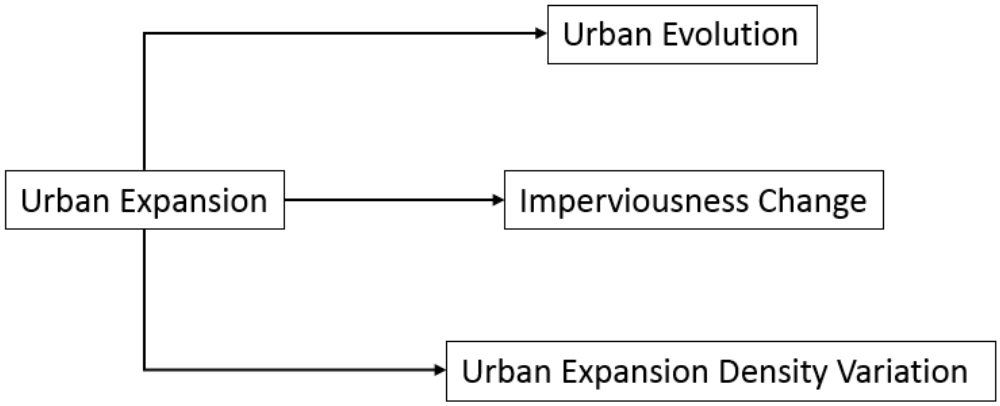

Fig. 1. Conceptualization Model.

3. Study area

The Ho Chi Minh City Metropolitan Area (Hereafter called HCMA), which lies in the Southeastern region of Vietnam and 1,760 km South of the capital Hanoi, was selected as our research area (Fig. 2). It has a tropical savanna climate with a dry (from November to April) and a wet season (from May to October). Despite these two distinguishable seasons, there is much less temperature fluctuation in the HCMA area than northern Vietnam. The proximate urban extent of the HCMA defined in this study is 5,004 km^2. Founded in 1698, this city began with approximately 20,000 Vietnamese migrants from the Central and Northern region in the 1623-1698 period ("The first 75 years", 2005). Due to continuing economic developments in agricultural and manufacturing production, the population of the HCMA increased to 5.03 million in 1999 and to 8.44 million in 2017 (General Statics of Vietnam). The urban population has also increased to 4.48 million in 2001 and to 6.68 million in 2015 (General Statistics Office of Vietnam). Thus far, the HCMA is the most populous urban agglomeration area in Vietnam. A wide variety of land cover types consist predominantly of developed urban lands, agricultural areas, production/special use forests, barren lands, and diverse waterbodies. Developed lands of the HCMA range from low density residential developments in the rural areas, to medium density residential settlements in the suburban areas, and higher density urban developments in the center city. The highest density urban settlements are focused on the inner urban core. In comparison, the rural areas possessing much sparser residential settlements are dominated by various types of agricultural lands. However, over 600 km^2 of agricultural areas have been converted for urban land uses from 1990 to 2012 (Kontgis et al., 2014). The study area has also encountered tremendous urban expansions and densifications. Therefore, the rapidly growing

urbanization and diverse land cover types in the HCMA makes it an ideal research area to analyze fast-paced changes in prospering megacities.

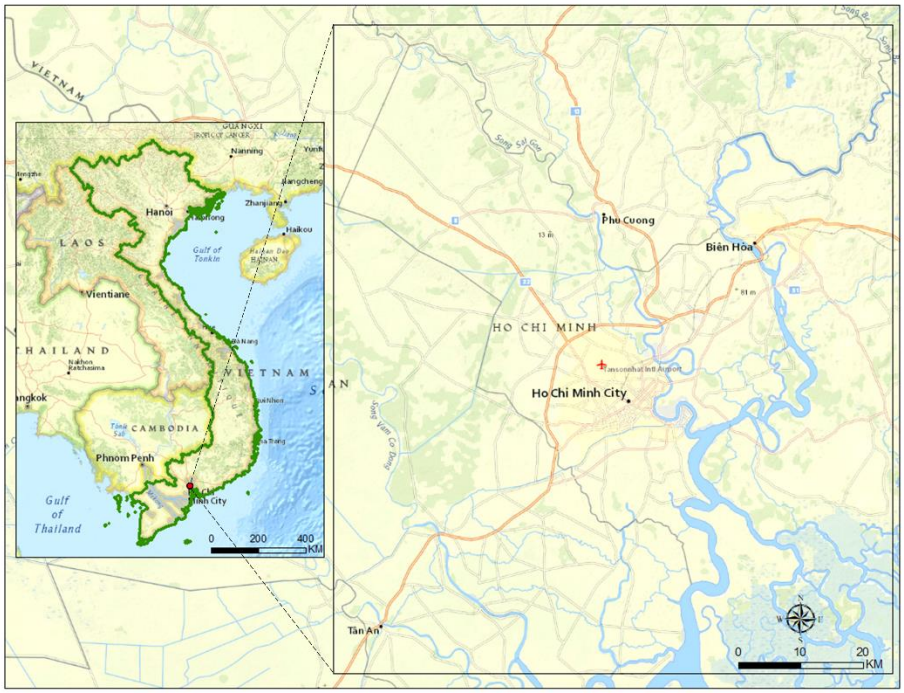

Fig. 2. Study area: Ho Chi Minh City Metropolitan Area (HCMA), Vietnam.

4. Data

The HCMA is located within two Landsat scenes (WRS-2: 125/52 and 125/53), delineated in Fig. 4G. Beginning in January 2008, the USGS and NASA implemented a new data distribution policy that provides Landsat data for free. Therefore, all Landsat data will be collected from the United States Geologic Survey Landsat data archive without any costs. Thus, all available Landsat images taken between 2000 and 2017 were ordered and obtained from the U.S. Geological Survey (USGS) online archive. It is worth noting that the HCMA has one of the severest cloud coverage due to its consistent high temperature and humidity. A majority of Landsat image qualities are significantly reduced by clouds and cloud shadows, whereas images with less than 20% cloud coverage can rarely be found (Fig. 4A-F). Therefore, collecting as many as Landsat images becomes essential for mapping sub-pixel urban impervious surface in this study. In total, 1,004 pre-processed Landsat images by USGS were downloaded and utilized, including the Thematic Mapper (TM), Enhanced Thematic Mapper Plus (ETM+), and Operational Land Imager (OLI). Their temporal distribution is shown in Fig. 3.

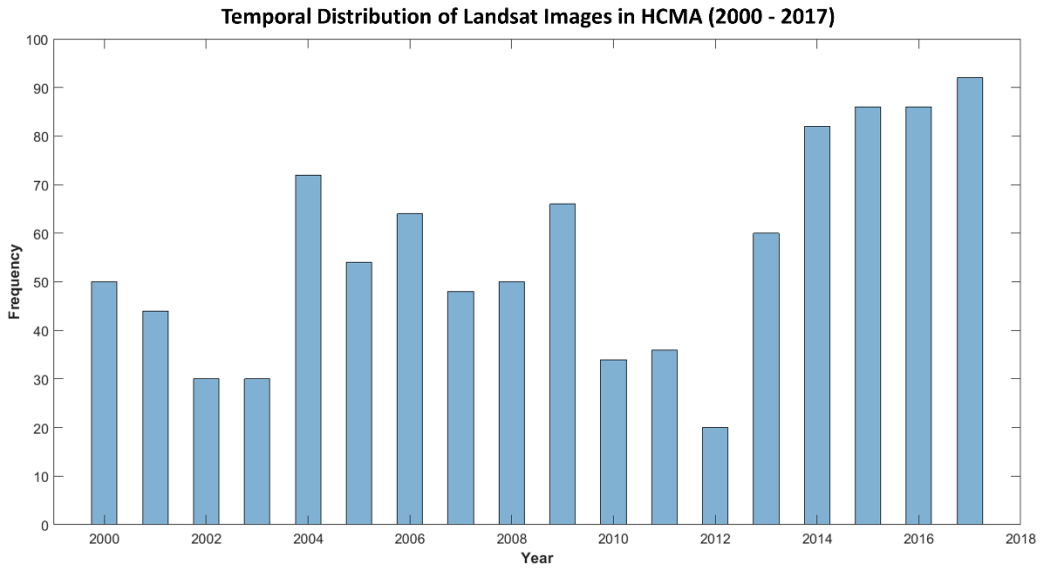

Fig. 3. Temporal distribution of used Landsat images.

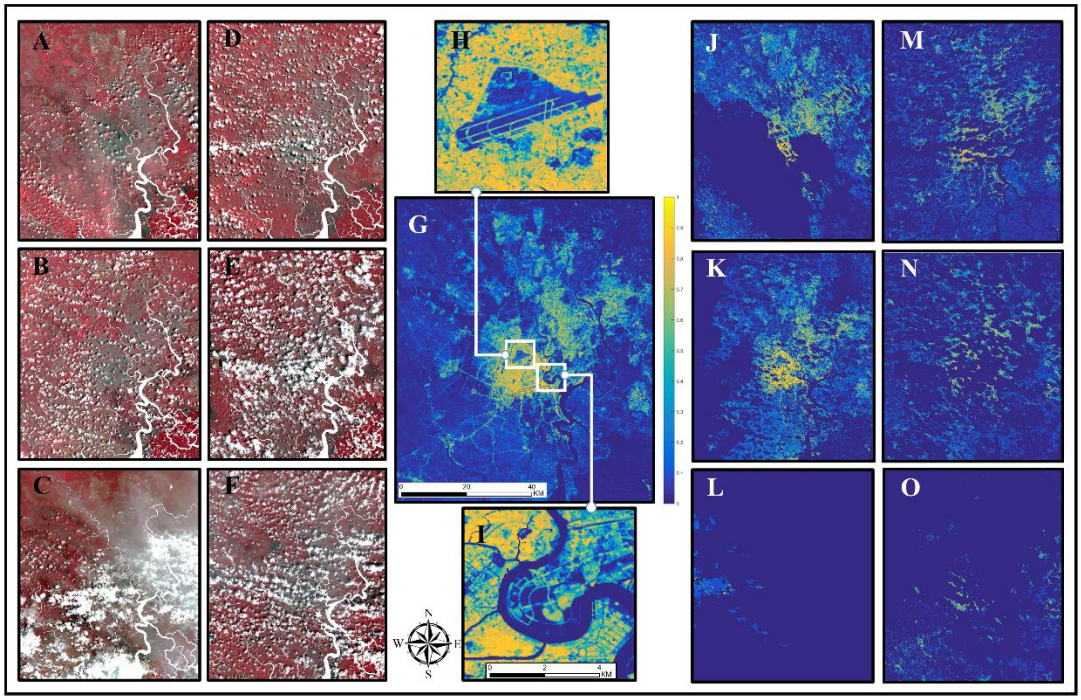

Fig. 4. Tropical savanna climate produces frequent dense clouds coverage over HCMA (Fig. 4A-F). Fmask algorithm is used to remove cloud and cloud shadows (Fig. 4J-O). Fig. 4G shows the

2016 HCMA urban impervious surface fraction map, and Fig. 4H&I are two close-ups of Tan Son Nhat International Airport and Thủ Thiêm New Urban Area.

5. Methodology

The methodology in this study contains several major steps: (1) image preprocessing; (2) training data collection; (3) random forest regression; (4) time series urban growth trajectory; (5) accuracy assessments; (6) urban expansion density modeling. Fig. 5 illustrates the framework of the methodology.

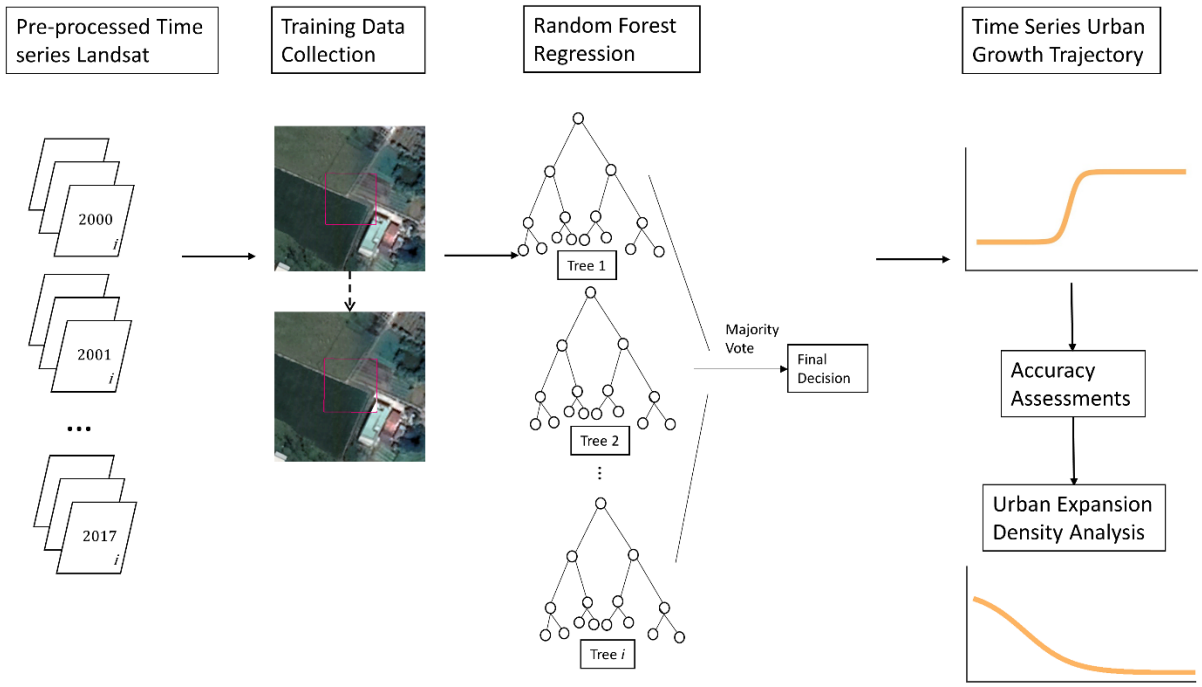

Fig. 5. Framework of the methodology in this study.

5.1 Image pre-processing

To derive surface reflectance data, the Landsat TM and ETM+ images were atmospherically corrected by the Landsat Ecosystem Disturbance Adaptive Processing System (LEADPS) (Schmidt et al., 2013), while the Landsat OLI images were processed using the

Landsat Surface Reflectance Code (LASRC) (USGS, 2018). The Universal Transverse Mercator grid system (UTM) – Zone 48 and World Geodetic System 1984 (WGS84) ellipsoid and datum were selected as the projected coordinate system. The Fmask algorithm was applied to remove pixels involving clouds or cloud shadows (Zhu & Woodcock, 2012) (Fig. 4J-O). In addition, reference information was properly generated through visual inspection and manual digitizing based on the historical collection of high-resolution satellite imagery from Google Earth.

5.2 Training data collection

A multi-temporal training dataset was performed to provide land cover training information for spectral change areas. This multi-temporal training dataset is consisting of samples drawn for every 3-5 years during the entire study period. Samples selected for previous years defined as unchanged in the subsequent period were ensured to be included in the sample pool for further training considerations. Initially, 800 randomly stratified training samples were manually digitized without considering seasonal impacts under the local tropical climate. Over 500 samples remained after the removal of invalid points falling in water bodies or under clouds and cloud shadows. Impervious surface cover fraction within each pixel was obtained and used as the dependent variable during modeling process.

5.3 Random forest regression

A total of six spectral reflectance bands (TM/ETM+: Bands 1-5, and 7; OLI: Bands 2-7) of each Landsat scene were entered as independent variable inputs. Only six independent variables were chosen because extra inputs might increase noise during the predicting process. Different bands are good at detecting distinct types of land uses. The training data were then fitted to the random forest regression model to infer impervious surface cover fraction from

varying surface reflectance band entries. The main idea of the random forest model is to relate remote sensing or GIS variables to percent imperviousness in the regression analysis for sub-pixel estimation of impervious surface cover. The random forest model was used by considering its robustness against overfitting and noise (Breiman, 2001). It has also been well-documented for its reliability and efficiency. Deng and Wu (2013) found that the random forest model could provide more satisfactory estimation results of percent imperviousness in highly heterogeneous study areas, compared to other classic machine learning methods. Specifically, random forest is an ensemble learning algorithm that grows many regression trees for improving the accuracy of prediction. Each time to estimate a new object, the model puts the input vector down each of the trees in the forest. After each tree generates a regression result (or we can say each tree has one vote), the forests choose the result having the most votes. Moreover, Random Forests does not overfit so that one can run as many regression trees as they want. This model is comprised of 4 principal steps: (1) randomly selecting samples with the bootstrap method from the original training sample set; (2) randomly selecting a set of independent variables from all variables; (3) Growing several classification trees without pruning by repeating step 1 and 2; (4) Selecting the finest results for the final prediction based on the votes (Breiman, 2001).

The fitted model was then applied to all available Landsat data from 2000 to 2017 to retrieve bimonthly impervious surface cover estimates. This generated a preliminary sub-annual stack of fractional urban impervious surface cover over the HCMA area. Its spatial and temporal resolution is 30 m * 30 m and 16 days, respectively. Time series clear observations were obtained using the Fmask algorithm (Zhu and Woodcock, 2012) (Fig. 4J-O). Overall, this sub-annual data stack should provide an impervious surface percentage of any clear-sky pixel for all available Landsat images on a bimonthly basis between 2000 and 2017. To generate this

information, over six computers in the lab were used for model constructions and percent imperviousness estimations. Finally, an annual stack of impervious surface fraction median composite layers based on the preliminary data stack was generated for modeling urban evolution and urban expansion density variations.

5.4 Time series urban growth trajectory

One of the most obvious technique for urban land cover change detection is the post-classification comparison (Singh, 1989). Popular methods of post-classification comparison include visual inspection and image differencing. However, these two means can lead to the missing of significant urban transition details in the temporal context because of the uncertain length of the urban land cover change process within a pixel. As a result, a post-classification method (Song et al., 2016) was conducted to reveal a complete historical profile of urban growth transition over the HCMA area. A typical long-term urban growth trajectory is composed of three phases: (1) early stable phase with no changes; (2) change phase with sharp or slow increase; (3) post-change phase with saturated impervious surfaces. This three-stage progress can be described using a four-parameter logistic model (Fig. 6):

$$IS(x) = \frac{a-d}{1+e^{c-bx}} + d \quad (1)$$

where IS is impervious surface, x is a julian year, d is the pre-change IS fraction (lower asymptote), a is the post-change IS fraction (upper asymptote), $a - d$ is the magnitude of change, and b and c control the slope and timing of change, respectively. This four-parameter logistic model was fitted to impervious surface time series of 8,900,032 pixels over the HCMA area. RMSE and adjusted R^2 were generated to estimate the resulting models' goodness of fit. Only statistically significant models with adjusted $R^2 > 0.3$ were saved for further research

analysis. High-resolution aerial imagery was added at significant time points for detailed urban transition illustration.

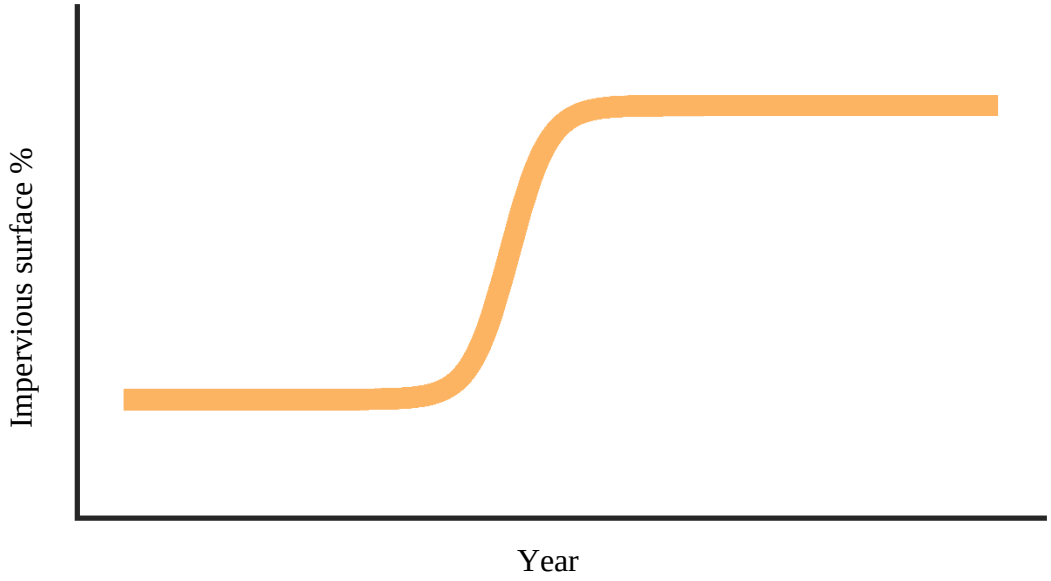

Fig. 6. An illustration of a four-parameter logistic model which indicates three distinct stages during urban growth events.

5.5 Accuracy assessments

Randomly stratified independent testing samples were used to evaluate the annual urban impervious surface fraction layers. Eight hundred test samples were drawn within the study area extent. Each sample reached to 90 m * 90 m to avoid any geometric error. They were then digitized based on high-resolution aerial photographs. Moreover, scatterplots were drawn to validate the estimate urban impervious surface fraction using testing sample data. The ground reference and the random forest prediction of impervious surface percentage were compared in 2002, 2006, 2009, 2012 and 2016. Three error indicators, RMSE, Mean Absolute Error (MAE) and Systematic Error (SE), were used to compute the per-pixel error and systematic bias of each scatterplot (Eq. 2-4). The adjusted R^2 value was also calculated.

$$RMSE = \sqrt{\frac{1}{n}\sum_{i=1}^{n}(\widehat{y_i} - y_i)} \quad (2)$$

$$MAE = \frac{1}{n}\sum_{i=1}^{n}|\widehat{y_i} - y_i| \quad (3)$$

$$SE = \frac{1}{n}\sum_{i=1}^{n}(\widehat{y_i} - y_i) \quad (4)$$

where, $\widehat{y_i}$ denotes the predicted impervious surface cover fraction for the ith pixel using the Random Forest model, y_i denotes the ground truth impervious surface cover fraction for the ith pixel, and n denotes the total number of the testing samples.

5.6 Urban expansion density modeling

By considering the most inner urban core in 2000 as the center, numerous 1-km buffers were created in an increasing manner extending outwards. The 6-km, 15-km, and 32-km buffer rings have been bolded as the urban, suburban, and agricultural boundary, respectively based on visual interpretation. After the city was partitioned into many concentric rings, zonal mean impervious surface fraction was extracted from each one of them. The concentric partitioning of the study area in 2017 is illustrated in Fig. 7. Also, impervious surface density variations over distance from the urban center were derived in multiple years, including 2001, 2004, 2007, 2010, 2013, and 2017. To analyze urban expansion density, a different logistic model was utilized for the illustration purpose. This selected logistic model is in the form (Fig. 8):

$$IS(x) = \frac{a-d}{1+e^{b-cx}} + d \quad (5)$$

where IS is impervious surface, x is the distance measured in kilometers, d is the low density IS fraction at the urban boundary (lower asymptote), a is the high density IS fraction at the urban core (upper asymptote), $a - d$ is the magnitude of change, and b and c control the slope and timing of change, respectively. A slight difference in the forms of the equation 1 and 5 is the

shifted position of b and c. More differently in the curve illustrations, the urban expansion density model starts with a gradual decline stage instead of an early stable stage.

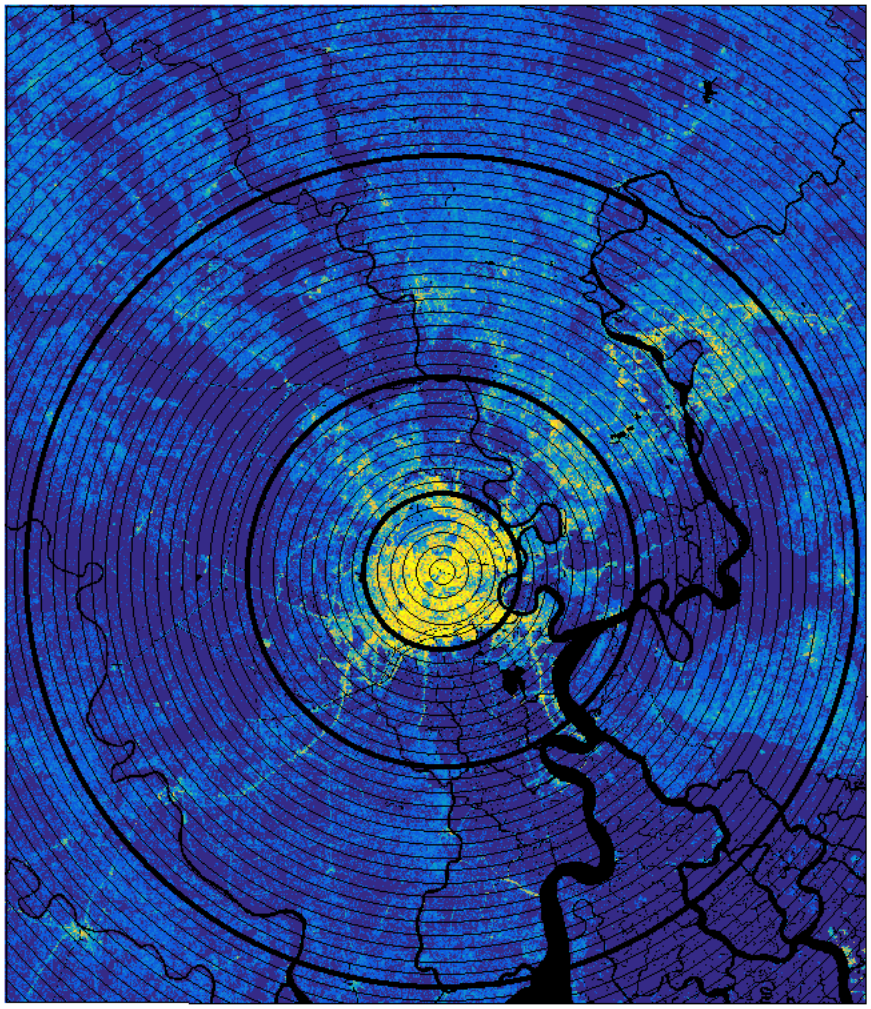

Fig. 7. The concentric ring partitioning of HCMA in 2000 (The three bolded buffer rings are the urban core boundary (6-km-radius), suburban boundary (15-km-radius), and the outer agricultural boundary (32-km-radius)).

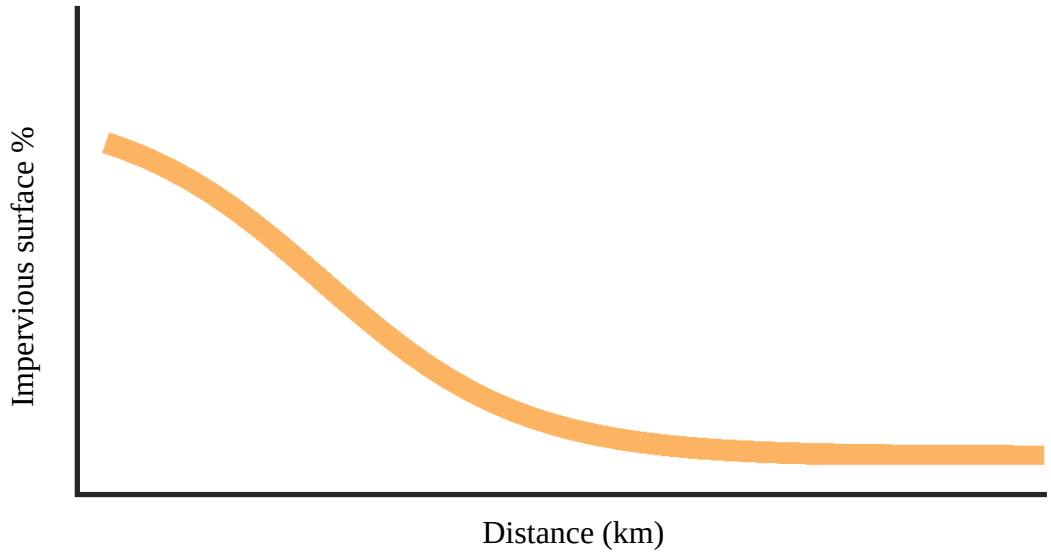

Fig. 8. An illustration of a four-parameter logistic model which indicates varying urban expansion density over distance.

6. Results and discussions

6.1 Annual stack of impervious surface cover fraction maps

The complete urban expansion process of the HCMA area between 2000 and 2017 is shown in Fig. 6. The annual impervious surface percentage was estimated as a continuously changing variable ranging from 0 to 100 over HCMA. The central urban density of HCMA (marked with bright yellow) continued to increase between 2000 and 2017 and caused great impacts in its surrounding provinces, including Binh Duong, Dong Nai, and Long An. The impervious surface fractions of non-urban land remained to be low (marked with blue). Newly converted urban land appeared to be in all directions of HCMA's urban core with continuing rising impervious surface values, but mainly in the Northeast and west (marked with cyan).

As shown in Fig. 6, in the northeastern direction, two towns (Thuận An and Dĩ An) and one city (Thủ Dầu Một) in Binh Duong province, and one city (Biên Hòa) in Dong Nai province was the earliest built-up area around HCMA since 2000. In the northern direction, Bến Cát rural district of Binh Duong started to be developed in 2003. In the further East, Biên Hòa city expanded southward along the national route QL 51 in Dong Nai province with intense industrial developments. To HCMA's West, two suburban districts (Củ Chi and An Tịnh) of HCMA were constructed since 2005 along QL 22 national route. Moreover, connected to the urban core of HCMA by the expressway CT01, Ben Luc town, Tan An city, and Đức Hòa Hạ rural district in Long An province were also converted to urban land in a fast pace. Compared against the other directions, relatively fewer developments were observed in the South because of its low altitude and proximity to the South China Sea. However, the Nhà Bè suburban district along the NHA

BE River down South in HCMA had intense urban developments through the study period. Finally, Ho 2 and Ha 2 are rejected and accepted, respectively because the HCMA area becomes increasingly expanded between 2000 and 2017.

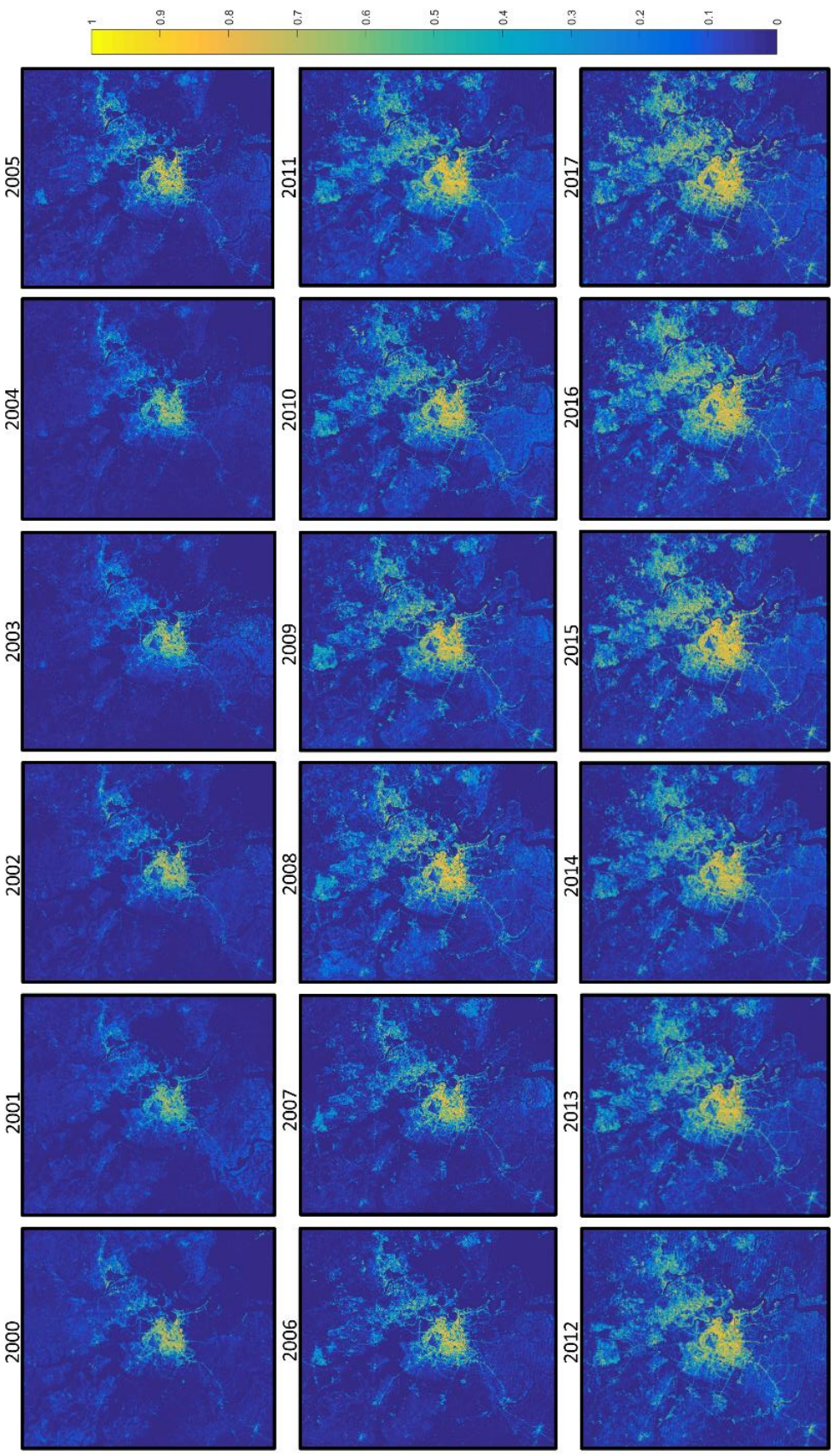
1
0.9
0.8
0.7
0.6
0.5
0.4
0.3
0.2
0.1
0
2000
2001
2002
2003
2004
2005
2006
2007
2008
2009
2010
2011
2012
2013
2014
2015
2016
2017

Fig. 9. Annual impervious surface estimates of HCMA between 2000 and 2017.

6.2 Urban impervious surface fraction at one point in time

The resultant 2017 sub-pixel impervious surface of the entire HCMA area is divided into three broad regions, including the urban, suburban, and agricultural. For comparison purposes, aerial imagery in corresponding regions are also provided. Fig. 10 indicate distinct spatial pattern types of urban, suburban and rural regions over HCMA. Fig. 10A shows a compact and dense urban area covered by high-intensity impervious surfaces in the center city. Dense urban area is labelled with bright yellowness whilst vegetated area is labelled with blueness. Different from Fig. 10A, Fig. 10D provides a natural-colored aerial imagery marking urban land use with silver and vegetated land with green. Both images denote that intensive impervious surface cover is concentrated over the urban area. Fig. 10A infers the areal proportion of impervious surface component at per-pixel basis, whereas Fig. 10D has proven not capable of inference. Moreover, Fig. 10B and 10E show illustrations of the suburban region at HCMA in which expanded but clustered urban settlements at fringes mixed with major transportation routes and fragmented cultivated lands. Fig. 10B, the sub-pixel impervious surface cover map precisely highlights the small-scale residential development areas surrounded by natural land areas. Furthermore, Fig. 10C and 10F demonstrate the rural agricultural regions with sparse residential developments and large scale of cropland. It is worth noting that impervious surface cover fraction maps of HCMA area at a per-pixel basis can provide indispensable information resources in governmental urban and environmental planning processes. First, most of the planning decisions are made based on multi-temporal urban analysis based on single or multiple Landsat imagery. Second, there is a lack in the availability of high-resolution imagery over the HCMA area, especially in the rural region. The earlier the data, the lower the availability is. Third, sub-pixel impervious surface

cover maps here can display small-scale urban settlements, fragmented agricultural land, and local transportation networks with high precision. Note that none of the ancillary datasets were included in our data.

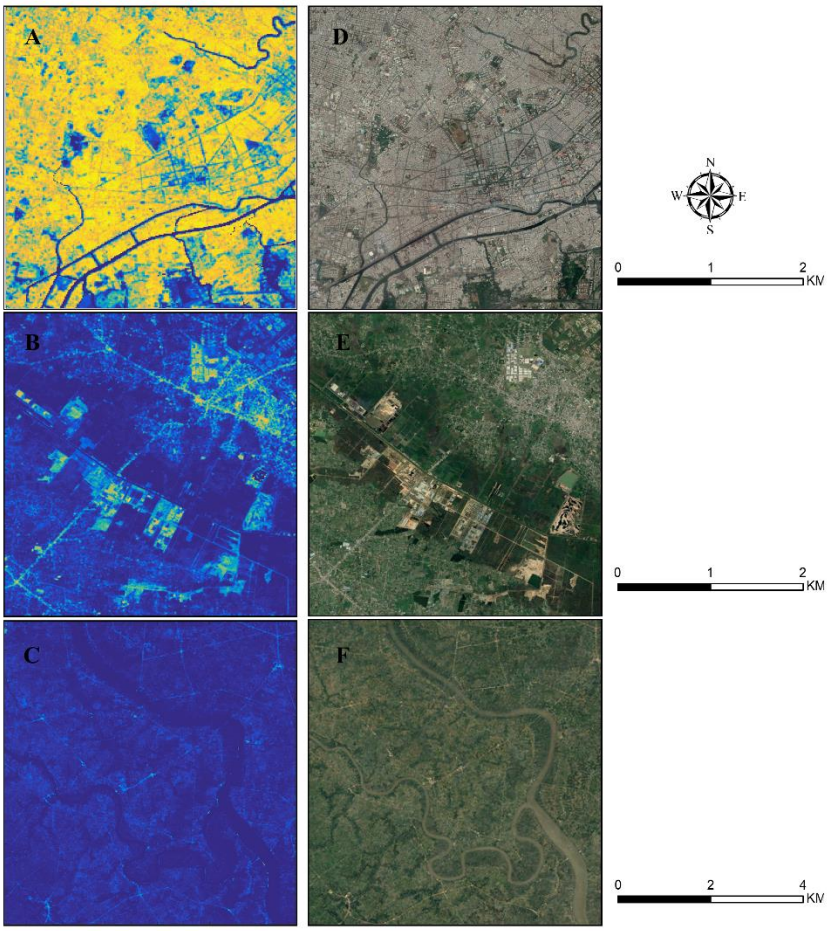

Fig. 10. Demonstration of percent impervious cover and aerial imagery in urban (A&D), suburban (B&E), and agricultural (C&F) regions.

6.3 Urban impervious surface fraction at multiple points in time

The HCMA area was zoomed in and its changing urban spatial patterns between 2000 and 2017 were illustrated in Fig. 11, 12, 13, and 14, respectively. In general, Fig. 11 and 12 are

captured with a view on a broader scale than Fig. 13 and 14. The former two illustrations demonstrate small-scale views of suburban regions, while the latter two demonstrate large-scale views detailed in pixels. Fig. 11 denotes Bien Hoa City neighboring Ho Chi Minh City in the northeast direction. This city is located in Dong Nai province. In 2000, it had a low impervious surface percentage with scattered residential settlements spreading along the local transportation roads (Fig. 11A). After 18 years, impervious surface significantly increased in Bien Hoa City in all directions (Fig. 11B). Its spatial pattern evolved from a "T" shape to a cross shape. The increase in urban developments at Bien Hoa City is also shown in Fig. 11C and 11D.

The major city demonstrated in Fig. 12 is Thu Dau Mot, which is the capital city of Bình Dương Province. This city becomes increasingly prosperous due to its adjacent location to the Ho Chi Minh City. It is located across the Saigon River to Ho Chi Minh City. As shown in Fig. 12, Impervious surface changed from low to high density between 2000 and 2017 in Thu Dau Mot City. Expanded urban developments have occurred in the North, West, and East.

Fig. 13 denotes the evolution process of Tan An City, the capital city in Long An province. Connected through the expressway CT01, Tan An city has developed at a fast pace under enormous effects from urbanization in Ho Chi Minh City. As shown in Fig. 13, radiative urban expansion has taken place in this city between 2000 and 2017. This city has a more complicated local transportation network and denser urban developments.

Duc Hoa Ha industrial district of Long An province locates adjacent to the urban boundary of Ho Chi Minh City. This area evolves from mainly agricultural land to highly intense impervious surfaces in the 2000-2017 period. As a result, this area appeared to be exceedingly fragmented with the complex industrial layout. Note that a water pond for industrial use was marked with 0-10% impervious surface cover fraction precisely.

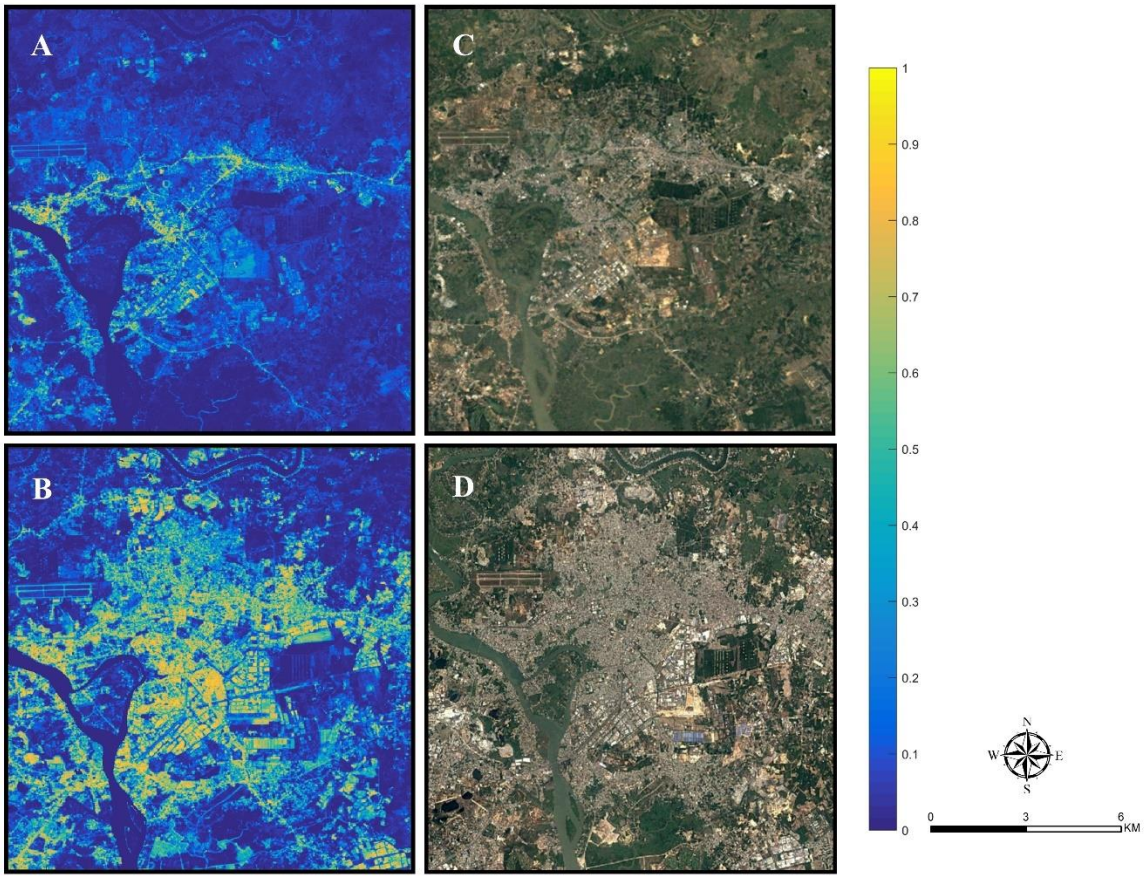

Fig. 11. Percent impervious surface increase in Bien Hoa City in HCMA: (A) 2000 Random forest modeled percent impervious surface; (B) 2017 Random forest modeled percent impervious surface; (C) 2000 Landsat/Copernicus aerial imagery; (D) 2017 Landsat/Copernicus aerial imagery.

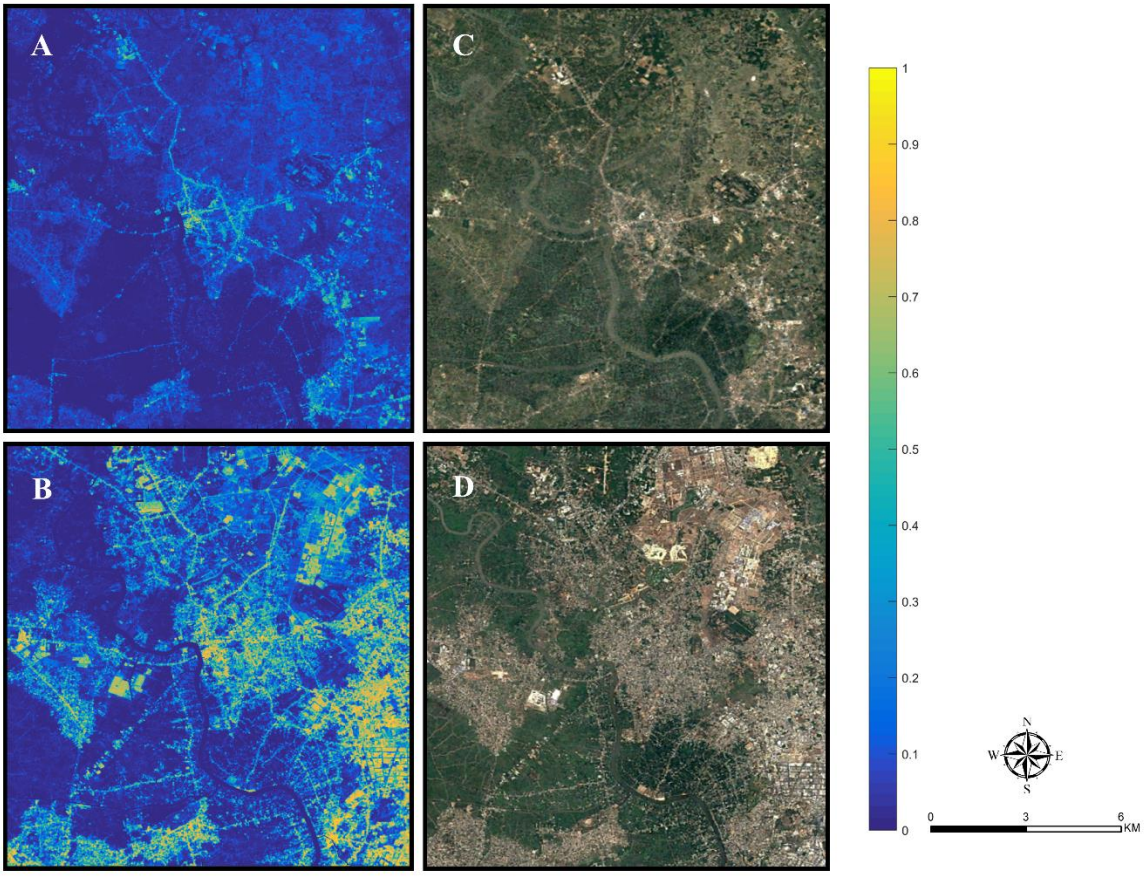

Fig. 12. Percent impervious surface increase in Thu Dau Mot City in HCMA: (A) 2000 Random forest modeled percent impervious surface; (B) 2017 Random forest modeled percent impervious surface; (C) 2000 Landsat/Copernicus aerial imagery; (D) 2017 Landsat/Copernicus aerial imagery.

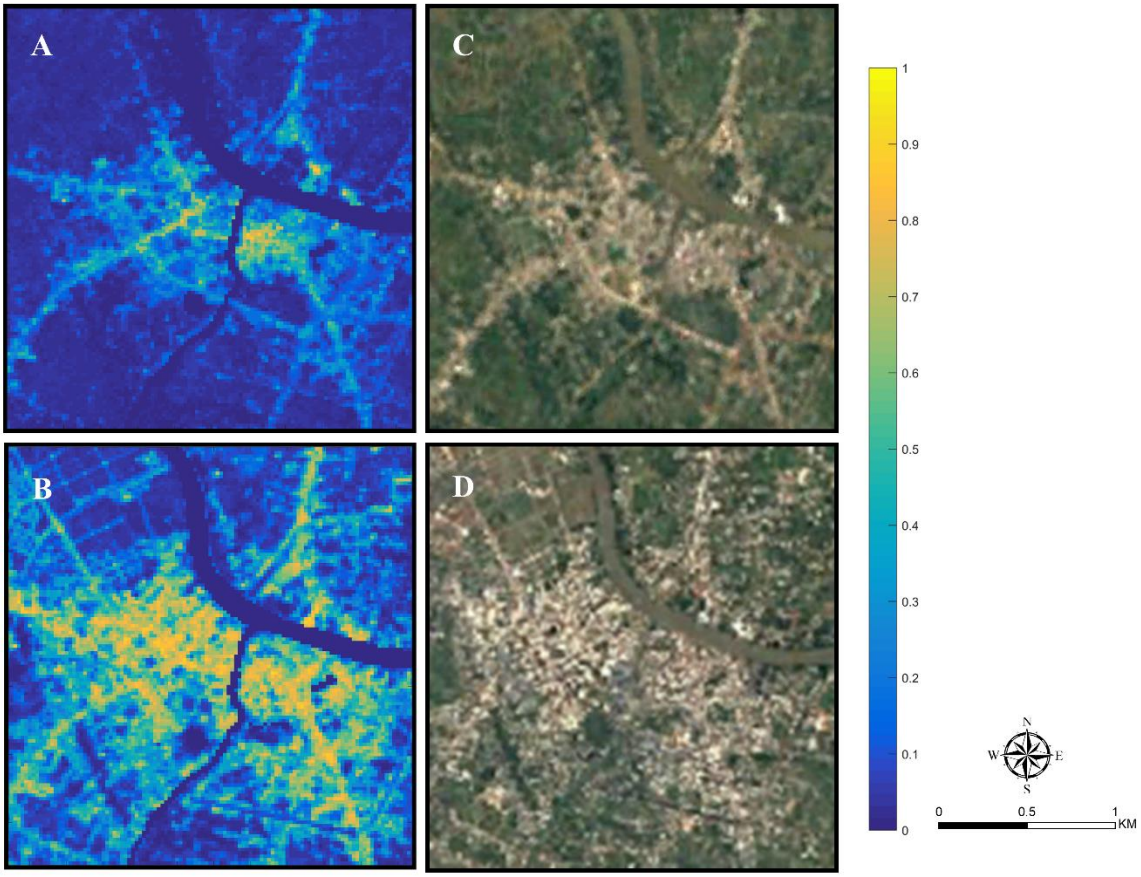

Fig. 13. Percent impervious surface increase in Tan An City in HCMA: (A) 2000 Random forest modeled percent impervious surface; (B) 2017 Random forest modeled percent impervious surface; (C) 2000 Landsat/Copernicus aerial imagery; (D) 2017 Landsat/Copernicus aerial imagery.

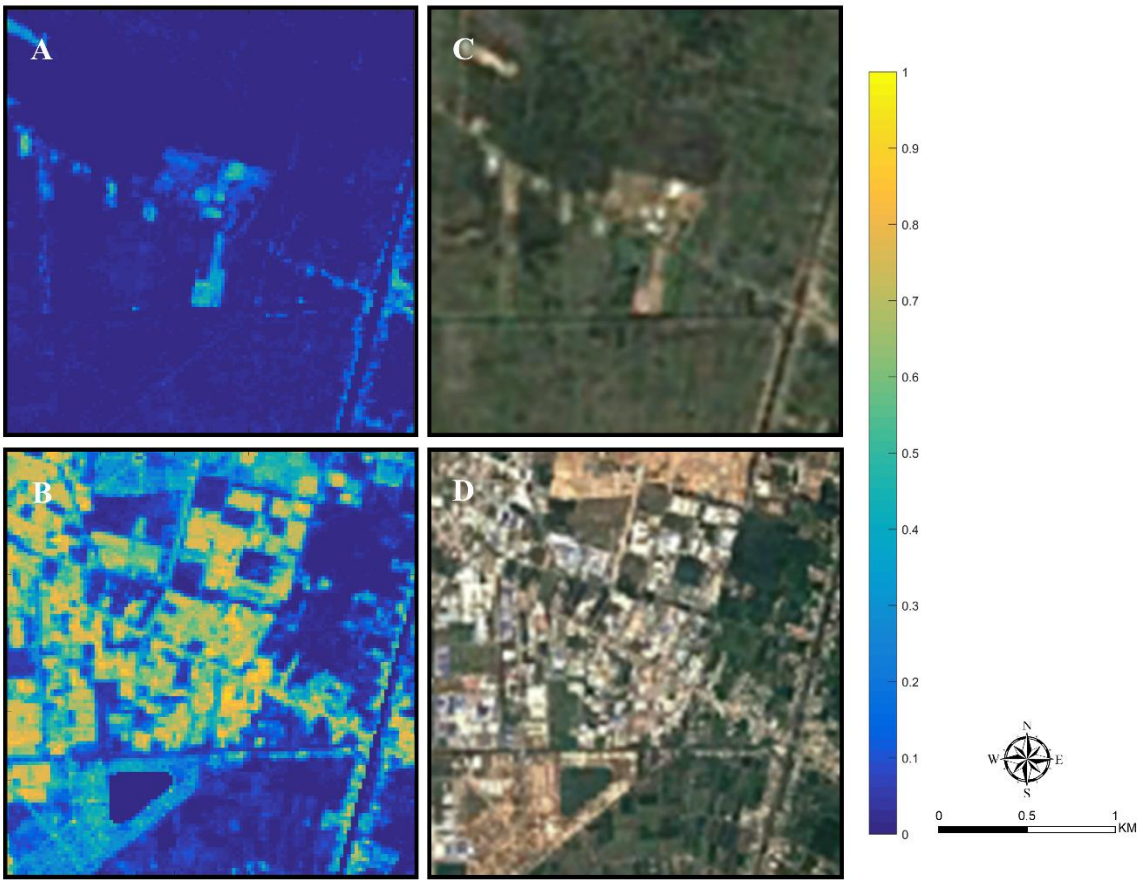

Fig. 14. Percent impervious surface increase in Duc Hoa Ha industrial district in HCMA: (A) 2000 Random forest modeled percent impervious surface; (B) 2017 Random forest modeled percent impervious surface; (C) 2000 Landsat/Copernicus aerial imagery; (D) 2017 Landsat/Copernicus aerial imagery.

6.4 Accuracy of modeled annual fractional impervious surface

Quantitative analysis was performed to measure the accuracy of impervious surface fraction estimates by using three important metrics, including MAE, SE, and RMSE. RMSE and MAE compute the per-pixel error, while SE quantifies the overall tendency of the systematic bias study area wise. In addition, adjusted R^2 is computed as a complementary metric for the

measurement of precision. Several scatterplots were derived by plotting the modeled impervious surface percentage against the reference percentage in 2002, 2006, 2009, 2012, and 2016 (Fig. 15). Impervious surface fractions are estimated well, especially in 2009, 2012, and 2016 (Fig. 15D-E) due to sample abundance. The accuracy seems acceptable with all adjusted R^2 over 0.8, RMSE less than or close to 10%, MAE less than 9%, the absolute SE values less than 0.9%, and slopes over 0.6. In general, all linear regression lines' slopes were over 0.6, while no intercept was more than 6%. Scatterplot 2002 has the highest adjusted R^2 (0.85) but the lowest regression slope (0.64). Scatterplot 2006 contains less scattered data points than the others due to insufficient available satellite imagery (Fig. 15B). Therefore, this year has the lowest intercept (2%), MAE (3.87%) and RMSE (5.02%). Scatterplot 2009 has the highest regression slope (over 0.7) among all (Fig. 15C). Scatterplot 2012 was observed with the lowest SE value (-0.04%). Excluding the computed accuracy metrics for 2006, the best MAE, SE, and RMSE estimates are 4.73%, 0.81%, and 5.52%, respectively. Also, the best value of adjusted R^2 is 0.85.

The accuracy of the adopted sub-pixel mapping method is comparable to, or even better than those of previous studies. The detailed comparisons are demonstrated in Table 1. One example is the annual, Landsat-based estimates of impervious cover of the Washington DC – Baltimore metropolitan region with an estimated MAE of 5.87%, an SE (referred to MBE in the text) of -3.5%, and an RMSE (referred to RMSD in the text) of 14.46% (Sexton et al., 2013). Another example is the annual impervious surface area mapping results in Jakarta Metropolitan Area, Indonesia, with an estimated RMSE of 20.31% and an R^2 of 0.60 (Tsutsumida et al., 2016). Ultimately, the newly developed continuous subpixel monitoring (CSM) method yielded a time series fraction cube in Broome County with an MAE of 4.60%, an SE of 0.20%, and an RMSE of 7.32%. All R^2 values are over 0.94. As a result, Ho 1 is rejected and Ha 1 is accepted that the

random forest model is a reliable and robust algorithm for mapping impervious surface cover at a sub-pixel spatial scale and time series temporal level.

Modeled IS% in Studies	**MAE (%)**	**SE (%)**	**RMSE (%)**	**R^2**
Washington DC-Baltimore Metropolitan Region (Song et al., 2016)	5.87	-3.5	14.46	N/A
Jakarta Metropolitan Region, Indonesia (Tsutsumida et al., 2016)	N/A	N/A	20.31	0.6
Broome County, New York, United States (Deng & Zhu, 2018)	4.6	0.2	7.32	0.94
Ho Chi Minh City Metropolitan Area, Vietnam	4.73	0.81	5.52	0.85

Table. Accuracy comparisons of modeled impervious surface cover fractions between the current study and three other studies. Metrics for the current study are highlighted with shade.

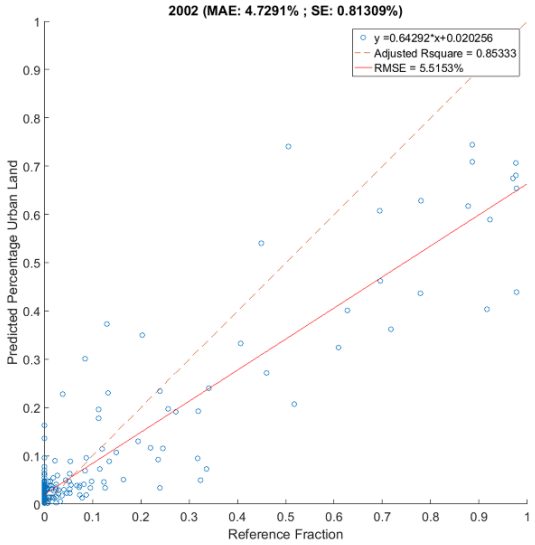
2002 (MAE: 4.7291% ; SE: 0.81309%)
y =0.64292*x+0.020256
Adjusted Rsquare = 0.85333
RMSE = 5.5153%
Predicted Percentage Urban Land
Reference Fraction

A

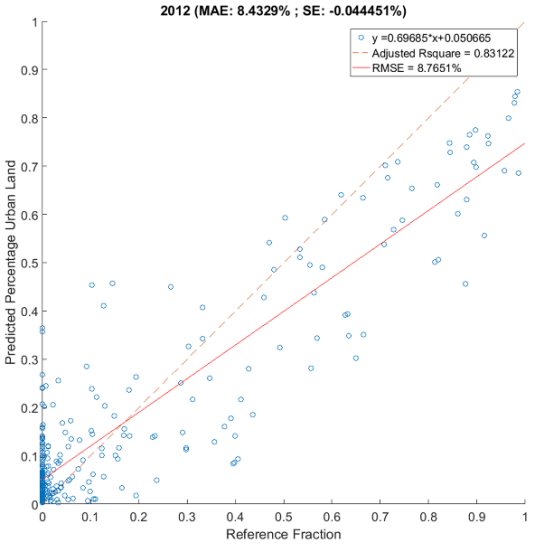
2012 (MAE: 8.4329% ; SE: -0.044451%)
y =0.69685*x+0.050665
Adjusted Rsquare = 0.83122
RMSE = 8.7651%
Predicted Percentage Urban Land
Reference Fraction

D

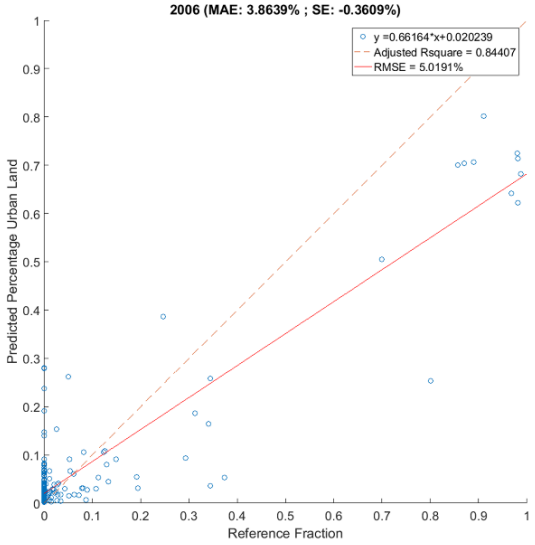
2006 (MAE: 3.8639% ; SE: -0.3609%)
y =0.66164*x+0.020239
Adjusted Rsquare = 0.84407
RMSE = 5.0191%
Predicted Percentage Urban Land
Reference Fraction

B

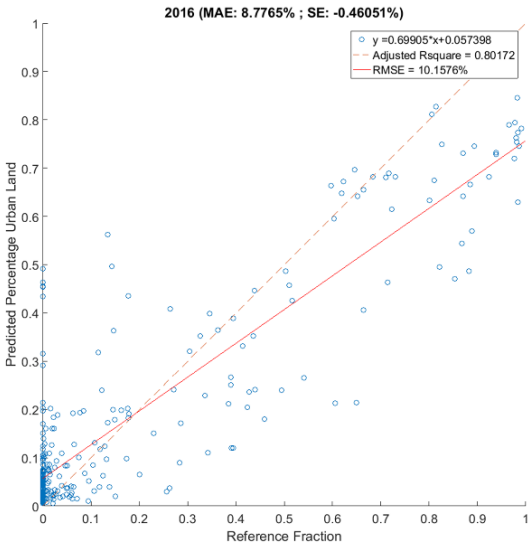
2016 (MAE: 8.7765% ; SE: -0.46051%)
y =0.69905*x+0.057398
Adjusted Rsquare = 0.80172
RMSE = 10.1576%
Predicted Percentage Urban Land
Reference Fraction

E

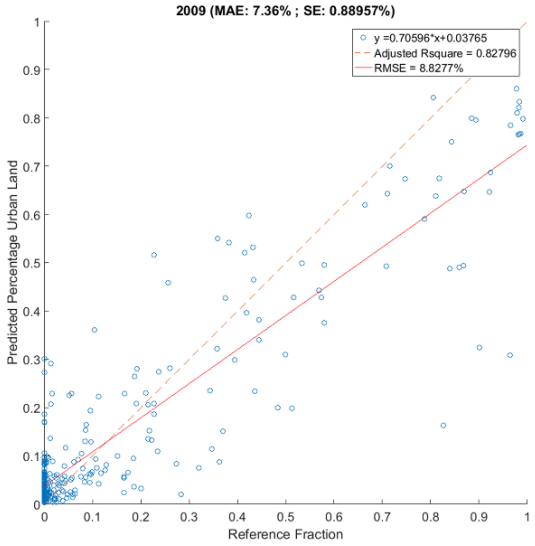
2009 (MAE: 7.36% ; SE: 0.88957%)
y =0.70596*x+0.03765
Adjusted Rsquare = 0.82796
RMSE = 8.8277%
Predicted Percentage Urban Land
Reference Fraction

C

Fig. 15. Scatterplots between modeled and reference urban impervious surface fraction in A) 2002, B) 2006, C) 2009, D) 2012, and E) 2016. The solid red line is the 1:1 reference line. The red dashed line is the linear regression line.

6.5 Time series urban growth trajectories

Due to intense urban expansion and densification trend over HCMA, all 8,900,032 pixels in the study area have been estimated with the proposed four-parameter logistic model (Eq. 1; Fig. 6). Models are fitted based on the annual medians of impervious surface cover fractions at HCMA. A representative long-term urban growth trajectory example is selected and shown in Fig. 16. The pink data points indicate the median impervious surface cover percentages of each year. A monotonically increasing urban transition process is delineated from the time series urban growth trajectory. A set of aerial imagery illustrations corresponding to the urban transition process is also demonstrated along with the curve.

Shown in Fig. 16, the pixel area changed from a pre-change phase with low impervious surface fraction, to a change phase with rapidly growing impervious surface fraction and a post-change phase with stable impervious surface fraction. Specifically, this pixel changed from agricultural (0% impervious surface fraction) in 2000 to urban land cover (50% impervious surface fraction) in 2009. It then remained to be stable through the rest of the study period. Among fitted models, the change phase has often occurred in the middle of the study period and lasted for 3 to 5 years during the urban growth events. Overall, this model presents a typical urban growth process with a satisfactory RMSE (2.87%) and nearly perfect adjusted R^2 (0.97). Hence, Ha 3 is accepted because urban expansion process over the HCMA area can be precisely demonstrated using a logistic model. Ho 3 is therefore rejected.

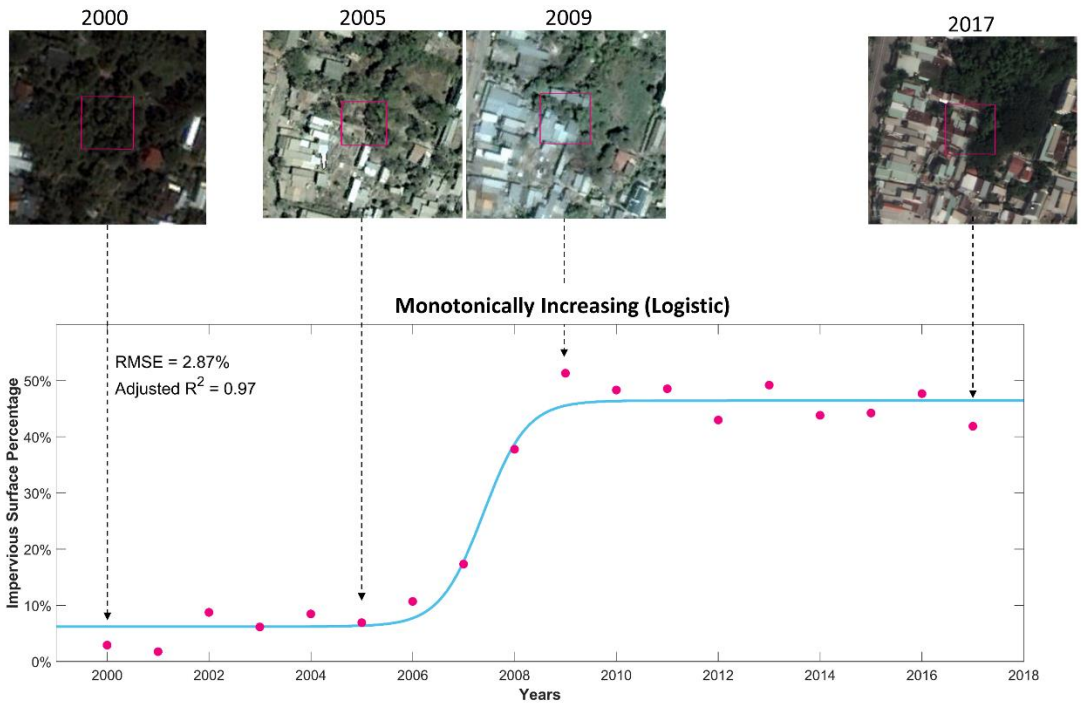

Fig. 16. A complete urban growth evolution process of a pixel is demonstrated using the four-parameter logistic model.

6.6 Urban expansion density analysis

The concentric-ring-based analysis quantified the spatiotemporal pattern of impervious surface density at HCMA. The urban density variations were examined using a logistic model (Eq. 5; Fig. 8). Delineated in Fig. 17, this fitted logistic model examines varying urban impervious surface cover density from the core to urban fringe. It also shows that impervious surface density, which was the highest at the urban core, continued to decrease as distance decayed from the center. This distance decay process includes three stages, including a gradual decline of density from the center to suburbs, a sharp drop from suburbs to rural areas, and a stable final stage with the lowest density. However, the geographical extents of the urban core, suburban, and rural divisions continued to change because of the rapid urban expansion throughout the study period. For comparative analysis here, the area boundaries of the urban

center, suburbs, and rural areas were defined as 0-6 km, 7-15 km, and 16-32 km. From 2000 to 2017, the impervious surface density of the urban center, suburbs, and rural areas increased 16.4%-31.6%, 14.8%-33.6%, and 6.7%-12.6%, respectively. The center city was rapidly densified under urban developments. Simultaneously, developments continued to sprawl towards suburbs and rural areas along major transportation routes. The radii of the center and suburban regions both grew at the expense of cropland loss in the rural area. Overall, Fig. 9 reveals that HCMA became more expanded during rapid urban expansion, though its center city became more densified and compact between 2007 and 2017. The accuracy of model fitting was assessed with satisfactory estimates of RMSE (1.24%-1.99%) and adjusted R^2 (0.99). Therefore, Ha 4 is accepted because there is a close relationship between urban expansion density and distance at the HCMA area. Ho 4 is thus rejected.

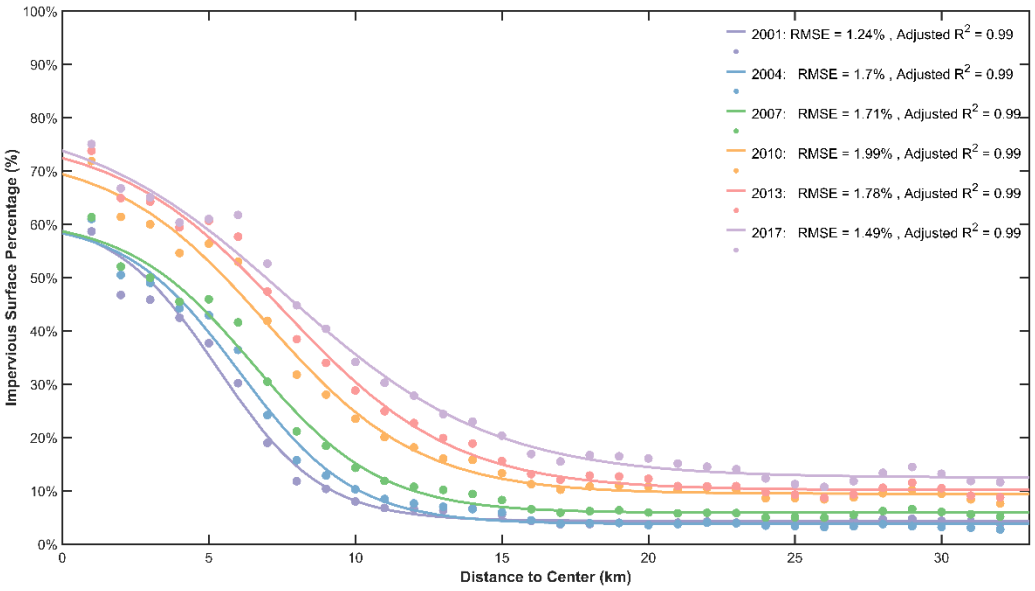

Fig. 17. Spatiotemporal patterns of urban expansion density over distance at HCMA.

7. Conclusion

An integrated approach was developed to map annual urban impervious surface cover fractions and analyze the long-term urban growth over HCMA using Landsat time series between 2000 and 2017. Various spectral information from each clear-sky training pixel was extracted in the past eighteen years. A group of selected spectral band values from training pixels were then employed as an input of the random forest regression for the inference of impervious surface cover fraction. Ultimately, the spatial and temporal contexts were incorporated to generate an annual, long-term, and horizontal view of urban growth with a long-term impervious surface fraction trajectory.

The annual, long-term, and continuous fields of impervious surface cover fraction estimation have shown that the HCMA area has undergone an accelerated growth in impervious surface area between 2000 and 2017. The urban area mainly extended from the center city to the Northeast and West directions. In these directions, large scales of agricultural land surrounding the suburban districts have been converted to urban land uses. On a basis of the generated proportional impervious surface cover results, urban growth models have been fitted to provide changing magnitude, timing, duration of the urbanization at HCMA. Effective time-series urban evolution analysis in the aspects of magnitude, timing, and duration of the change can be highly beneficial in governmental urban and environmental planning decision-making processes. Sub-pixel scaled long-term impervious surface cover fraction estimations can also provide indispensable data about varying urbanization extents at HCMA. Additionally, the urban

expansion density over distance from the urban core was quantified based on a concentric ring partitioning analysis. The urban, suburban, and agricultural regional divisions have changed enormously due to massive urban expansion between 2000 and 2017. Spatially, the urban division with high-density residential and business developments has been densified under continuing urban growth at HCMA. The suburban region with mostly medium-density urban developments has experienced fast-paced urban expansion and continued to push its boundary towards upon the agricultural area with mainly low-density developments.

8. References

1. Arnold, C.L., Boison, P.J., Patton, P.C., 1982. Sawmill Brook: An Example of Rapid Geomorphic Change Related to Urbanization. J. Geol. 90(2), 155-166.
2. Arnold, C.L., Gibbons, C.J., 1996. Impervious surface coverage: the emergence of a key environmental indicator. J. Am. Plan. Assoc. 62, 243-258.
3. Barbec, E., Schulte, S., Richards, P.L., 2002. Impervious surface and water quality: a review of current literature and its implications for watershed planning. J. Plan. Lit. 16(4), 499-514.
4. Bagan, H., Yamagata, Y., 2014. Land-cover change analysis in 50 global cities by using a combination of Landsat data and analysis of grid cells. Environ Res Lett. 9, 1-13.
5. Breiman, L., 2001. Random forests. Mach. Learn. 45, 5-32.
6. d'Amour, C., Reitsma, F., Baiocchi, G., Barthel, S., Güneralp, B., Erb, K.-H., … Seto, K. C., 2017. Future urban land expansion and implications for global croplands. Proc Natl Acad Sci USA. 114(34), 8939–8944.
7. Burns, D., Hassett, J., Duncan, J., Kendall, C., Vitvar, T., and McDonnell, J., 2005. Effects of suburban development on runoff generation in the Croton River Basin, New York, USA. J. Hydrol. 311(1-4), 266-281.
8. Chabaeva, A., Civco, D.L., Hurd, J.D., 2009. Assessment of impervious surface estimation techniques. J. Hydrol. Eng. 14, 377-387.
9. d'Amour, C.B., Reitsma, F., Baiocchi, G., Barthel, S., Güneralp, B., Erb, K., Haberl, H., Creutzig, F., Seto, K., 2017. Future urban land expansion and implications for global croplands. Proc Natl Acad Sci USA. 114(34), 8939-8944.

10. DeFries, R.S., Rudel, T., Uriarte, M., Hansen, M., 2010. Deforestation driven by urban population growth and agricultural trade in the twenty-first century. Nat. Geosci. 3, 178-181.
11. Deng. C., Zhu, Z., 2018. Continuous subpixel monitoring of urban impervious surface using Landsat time series. Remote Sens. Environ. In press.
12. Deng, C., Wu, C., 2013a. A spatially adaptive spectral mixture analysis for mapping subpixel urban impervious surface distribution. Remote Sens. Environ. 133, 62-70.
13. Deng, C., Wu, C., 2013b. The use of single-date MODIS imagery for estimating large-scale urban impervious surface fraction with spectral mixture analysis and machine learning techniques. ISPRS J. Photogramm. Remote Sens. 86, 100-110.
14. Deng, C., Li, C., Zhu, Z., Lin, W., Xi, L., 2017. Subpixel urban impervious surface mapping: the impact of input Landsat images. ISPRS J. Photogramm. Remote Sens. 133, 89-103.
15. Gnecco, I., Berretta, C., Lanza, L.G., Barbera, P.L., 2005. Storm water pollution in the urban environment of Genoa, Italy. Atmos. Res. 77(1-4), 60-73.
16. Homer, C., Dewitz, J., Yang, L., Jin, S., Danielson, P., Xian, G., Coulston, J., Herold, N., Wickham., J., Megown, K., 2015. Completion of the 2011 national land cover databases for the conterminous United States - Representing a decade of land cover change information. Photogramm. Eng. Remote. Sens. 81, 345-354.
17. Jennings, D.B., and Jarnagin, S.T., 2002. Changes in anthropogenic impervious surfaces, precipitation and daily streamflow discharge: a historical perspective in a mid-atlantic subwatershed. Landscape Ecol. 17(5), 471-489.
18. Lu, D., Moran, E., Hetrick, S., 2011. Detection of impervious surface change with multitemporal Landsat images in an urban-rural frontier. ISPRS J. Photogramm. Remote Sens. 66, 298-306.

19. Mallin, M.A., Williams, K.E., Esham, E.C., Lowe, R.P., 2000. Effect of human development on bacteriological water quality in coastal watersheds. Ecol Appl. 10(4), 1047-1056.
20. McKinney, M., 2006. Urbanization as a major cause of biotic homogenization. Bios. Cons, *127*(3), 247–260.
21. Melesse, A.M., Wang, X.X., 2008. Impervious surface area dynamics and storm runoff response. In Weng, Q. (Ed.), Remote sensing of impervious surface (pp. 369-386). Boca Raton, FL: CRC Press.
22. Miltner, R.J., White, D., Yoder. C., 2004. The biotic integrity of streams in urban and suburbanizing landscapes. Landsc. Urban Plann. 69, 87-100.
23. Moscrip, A.L., Montgomery, D.R., 1997. Urbanization, flood, frequency, and salmon abundance in Puget Lowland Streams. J Am Water Resour Assoc. 33(6), 1289-1297.
24. Montgomery, M., 2008. The urban transformation of the developing world. Sci, 319(5864), 761–763.
25. Novotny, V., 1994. Water quality: prevention, identification and management of diffuse pollution. New York: Van Nostrand-Reinhold Publishers.
26. Powell, R.L., Roberts, D.A., Dennison, P.E., Hess, L.L., 2007. Sub-pixel mapping of urban land cover using multiple endmember spectral mixture analysis: Manaus, Brazil. Remote Sens. Environ. 106, 253-267.
27. Powell, S.L., Cohen, W.B., Yang, Z., Pierce, J.D., Alberti, M., 2008. Quantification of impervious surface in the Snohomish Water Resources Inventory of Western Washington from 1972-2006. Remote Sens. Environ. 112, 1895-1908.

28. Ridd. M.K., 1995. Exploring a V-I-S (vegetation-impervious surface-soil) model for urban ecosystem analysis through remote sensing: comparative anatomy for cities. Int J Remote Sens. 16, 2165-2185.
29. Sartor, J.D., Boyd, G.B., 1972. Water pollution aspects of street surface contaminants. Washington, D.C.: Environmental Protection Agency.
30. Schuler, T.R., 1994. The importance of imperviousness. Watershed Prot. Tech. 1(3), 100-111.
31. Schuler, T.R., 2003. Impacts of impervious cover on aquatic systems. Watershed protection research monograph No.1. Center for Watershed Protections, Ellicot City, MD.
32. Schneider, A., Mertes, C.M., Tatem, A.J., Tan, B., Sulla-Menashe, D., Graves, S.J., Patel, N.N., Horton, J.A., Gaughan, A.E., Rollo, J.T., Schelly, J.T., Stevens, F.R., Dastur, A., 2015. A new urban landscape in East-Southeast Asia, 2000-2010. Environ Res Lett. 10, 1-14.
33. Schmidt, G., Jenkerson, C., Masek, J., Vermote, E., Gao, F., 2013. Landsat ecosystem disturbance adaptive processing system (LEDAPS) algorithm description. In: Openfile Rep. 2013-1057, 1-27.
34. Sexton, J.O., Song, X.P., Huang, C., Channan, S., Baker, M.E., Townshend, J.R., 2013. Urban growth of the Washington, D.C.-Baltimore, MD metropolitan region from 1984 to 2010 by annual, Landsat-based estimates of impervious cover. Remote Sens. Environ. 129, 42-53.
35. Seto, K., Guneralp, B., Hutyra, L., 2012. Global forecasts of urban expansion to 2030 and direct impacts on biodiversity and carbon pools. Proc Natl Acad Sci USA. 109, 16083-16088.
36. Seto, K., Shepherd, J., 2009. Global urban land-use trends and climate impacts. Curr. Opin. Environ. Sustain. 1, 89-95.

37. Shatahmassebi, A.R., Song, J., Zheng, Q., Blackburn, G.A., Wang, K., Huang, L.Y., Pan, Y., Moore, N., Shahtahmassebi, G., Haghighi, R.S., Deng, J.S., 2016. Remote sensing of impervious surface growth: A framework for quantifying urban expansion and re-densification mechanisms. Int. J. Appl. Earth Obs. Geoinf. 46, 94-112.
38. Song, X.P., Sexton, J.O., Huang, C., Channan, S., Townshend, J.R., 2016. Characterizing the magnitude, timing and duration of urban growth from time series of Landsat-based estimates of impervious cover. Remote Sens. Environ. 175, 1-13.
39. Sodhi, N., Koh, L., Brook, B., Ng, P. K., 2004. Southeast Asian biodiversity: an impending disaster. Trends. Ecol. Evol. 19(12), 654–660.
40. Taubenböck, H., Esch, T., Felbier, A., Wiesner, M., Roth, A., Dech, S., 2012. Monitoring urbanization in mega cities from space. Remote Sens. Environ. 117, 162-176.
41. Tong, S.T.Y., Chen. W., 2002. Modeling the relationship between land use and surface water quality. J. Environ. Manage. 66, 377-393.
42. Tsutsumida, N., Comber, A., Barrett, K., Saizen, I., Rustiadi, E., 2016. Sub-pixel classification of MODIS EVI for annual mappings of impervious surface areas. Remote Sens. 8(2), 143-161.
43. The first 75 years. 2015. Retrieved from http://www.eng.hochiminhcity.gov.vn/abouthcmcity/Lists/Posts/AllPosts.aspx?CategoryId=9
44. Xian, G., Crane, M., Su, J., 2007. An analysis of urban development and its environmental impact on the Tampa Bay watershed. J. Environ. Manage. 85, 965-976.
45. United Nations, 2008. World Urbanization Prospects: The 2008 Revision, New York: United Nations Population Division.

46. United Nations, 2018. World Urbanization Prospects: The 2018 Revision, New York: United Nations Population Division.

47. Van der Werf, G., Morton, D., DeFries, R., Olivier, G., Kasibhatla, P., Jackson, R., Collatz, G., Randerson, J., 2009. CO_2 emissions from forest loss. Nat. Geosci. 2, 737-738.

48. Ward, D., Phinn, S.R., Murray, A.T., 2000. Monitoring growth in rapidly urbanizing areas using remotely sensed data. Prof Geogr. 52(3), 371-386.

49. World Bank, 2011. Vietnam Urbanization Review: Technical Assistance Report.

50. Gilles, R.R., Box, J.B., Symanzikc, J., Rodemaker, E.J., 2003. Effects of urbanization on the aquatic fauna of the line creek watershed, Atlanta - A satellite perspective. Remote Sens. Environ. 86, 411-422.

51. Wu, C., 2004. Normalized spectral mixture analysis for monitoring urban composition using ETM+ imagery. Remote Sens. Environ. 93, 480-492.

52. Xian, G., Crane, M., 2005. Assessments of urban growth in the Tampa Bay watershed using remote sensing data. Remote Sens. Environ. 97, 203-215.

53. Xian, G., Crane, M., McMahon, C., 2008. Quantifying multi-temporal urban development characteristics in Las Vegas from Landsat and ASTER data. Photogramm. Eng. Remote. Sens. 74(4), 473-481.

54. Xian, G., Homer, C., 2010. Updating the 2001 national land cover database impervious surface products to 2006 using Landsat imagery change detection methods. Remote Sens. Environ. 114, 1676-1686.

55. Yang, L., Huang, C., Homer, C.G., Wylie, B.K., Coan, M.J., 2003a. An approach for mapping large-area impervious surfaces: synergistic use of Landsat-7 ETM+ and high spatial resolution imagery. Can J Remote Sens. 29, 230-240.

56. Yang, L., Xian, G., Klaver, J.M., Deal, B., 2003b. Urban land-cover change detection through sub-pixel imperviousness mapping using remotely sensed data. Photogramm. Eng. Remote. Sens. 69(9), 1003-1010.

57. Yuan, F., Bauer, M.E., 2007. Comparison of impervious surface area and normalized difference vegetation index as indicators of surface urban heat island effects in Landsat imagery. Remote Sens. Environ. 106, 375-386.

58. Young, R.A., Onstad, C.A., Bosch, D.D., Anderson, W.P., 1989. AGNPS: A nonpoint-source pollution model for evaluating agricultural watersheds. J Soil Water Conserv. 44(2), 168-173.

59. Zhu, Z., Woodcock, C., 2012. Object-based cloud and cloud shadow detection in Landsat imagery. Remote Sens. Environ. 118, 83-94.

60. Zhu, Z., 2017. Change detection using Landsat time series: a review of frequencies, pre-processing, algorithms, and applications. ISPRS J. Photogramm. Remote Sens. 130, 370-384.